Membrane-Bound Conformation and Topology of the Antimicrobial Peptide Tachyplesin I by Solid-State NMR†

Tim Doherty,‡ Alan J. Waring,§ and M. Hong*,‡

Department of Chemistry, Iowa State University, Ames, Iowa 50011, and Department of Medicine, University of California, Los Angeles, California 90095

Received July 14, 2006; Revised Manuscript Received September 1, 2006

ABSTRACT: The conformation and membrane topology of the disulfide-stabilized antimicrobial peptide tachyplesin I (TP) in lipid bilayers are determined by solid-state NMR spectroscopy. The backbone (ϕ and ψ) torsion angles of Val_6 are found to be −133° and 142°, respectively, and the Val_6 CO−Phe_8 H^N distance is 4.6 Å. These constrain the middle of the N-terminal strand to a relatively ideal antiparallel β-sheet conformation. In contrast, the ϕ angle of Gly_{10} is ±85°, consistent with a β-turn conformation. Thus, TP adopts a β-hairpin conformation with straight strands, similar to its structure in aqueous solution but different from a recently reported structure in DPC micelles where bending of the two β-strands was observed. The Val_6 and Gly_{10} CO groups are both 6.8 Å from the lipid ^{31}P, while the Val_6 side chain is in ^1H spin diffusion contact with the lipid acyl chains. These results suggest that TP is immersed in the glycerol backbone region of the membrane and is oriented roughly parallel to the plane of the membrane. This depth of insertion and orientation differs from those of the analogous β-sheet antimicrobial peptide protegrin-1 and suggest the importance of structural amphiphilicity in determining the location and orientation of membrane peptides in lipid bilayers.

Tachyplesin I (TP)[1] is a disulfide-linked 17-residue antimicrobial peptide produced from the hemocytes of the horseshoe crab *Tachyplesus tridentatus* (*1*). As a member of the antimicrobial peptide family, it is a component of the host defense system against microbial attacks (*2*). The interaction of TP with lipid membranes has been investigated in detail (*3*). It causes calcein leakage in phosphatidylglycerol-containing lipid vesicles (*4*) and forms anion-selective pores (*5*). In a process that is concomitant with pore formation, TP translocates across the membrane. At long times, the peptide micellizes the membrane, as shown by electron microscopy and light scattering experiments (*6*).

Despite much information about the membrane interaction of TP, a high-resolution structure of the peptide in lipid bilayers is so far unavailable. ^1H solution NMR studies of TP in water showed that TP has an antiparallel β-sheet conformation organized as a hairpin held by two cross-strand disulfide bonds, Cys_3−Cys_{16} and Cys_7−Cys_{12} (*7*, *8*). In a 320 mM dodecylphosphocholine (DPC) micelle solution, the peptide was found to undergo a significant conformational change where both the N- and C-terminal strands curl up around the middle of each strand (*8*) (PDB entry 1MA5). In contrast, in 60 mM DPC micelles, a straight β-hairpin conformation similar to the structure in water was found (*9*) (PDB entry 1WO1). This difference prompts the question of what the TP structure is in the most biologically relevant environment of lipid bilayers. In addition to the peptide conformation, the orientation and depth of insertion of TP also provide important insights into the mechanism of action of the peptide and have not been studied in detail.

In this work, we employ solid-state NMR spectroscopy to investigate the conformation and topology of TP in dimyristoylphosphatidylcholine (DMPC) bilayers and in mixed DMPC/dimyristoylphosphatidylglycerol (DMPG) membranes. Combining ϕ and ψ torsion angle measurements and distance experiments, we find that Val_6 and Cys_7, two residues in the middle of the N-terminal strand, adopt a canonical antiparallel β-sheet conformation, while Gly_{10} has a ϕ torsion angle consistent with a β-turn. Thus, no bending is observed in the β-strands in the lipid bilayer. We also determined the distances from the peptide to the lipid ^{31}P and to the lipid chain CH_2 protons. These data indicate that TP is immersed in the glycerol backbone region of the membrane in parallel to the plane of the membrane.

MATERIALS AND METHODS

Preparation of Membrane Samples. Isotopically labeled amino acids were purchased from Isotec (Miamisburg, OH) and Cambridge Isotope Laboratory (Andover, MA) and converted to Fmoc derivatives in house or by Synpep Corp. TP (NH_2-KWCFRVCYRGICYRRCR-$CONH_2$) was synthesized on an ABI 431A synthesizer using standard solid-phase

† This work is supported by National Institutes of Health Grants GM-066976 to M.H. and AI-37945 to A.J.W.

* To whom correspondence should be addressed: Department of Chemistry, Iowa State University, Ames, IA 50011. Telephone: (515) 294-3521. Fax: (515) 294-0105. E-mail: mhong@iastate.edu.

‡ Iowa State University.

§ University of California.

[1] Abbreviations: TP, tachyplesin I; PG-1, protegrin-1; DMPC, 1,2-dimyristoyl-*sn*-glycero-3-phosphatidylcholine; DMPG, 1,2-dimyristoyl-*sn*-glycero-3-phosphatidylglycerol; POPC, 1-palmitoyl-2-oleoyl-*sn*-glycero-3-phosphatidylcholine; POPE, 1-palmitoyl-2-oleoyl-*sn*-glycero-3-phosphoethanolamine; POPG, 1-palmitoyl-2-oleoyl-*sn*-glycero-3-phosphatidylglycerol; DPC, dodecylphosphocholine.

10.1021/bi061424u CCC: $33.50
Published on Web 10/17/2006

methods as described previously (*10*). The purity of TP was greater than 95% on the basis of analytical HPLC.

Isotopically labeled TP was reconstituted into lipid membranes by mixing the peptide solution and the lipid vesicle solution above the phase transition temperature of the lipids. A peptide:lipid molar ratio of 1:15 was used for all samples, to obtain sufficient sensitivity for the NMR experiments. Either a neutral DMPC membrane or an anionic DMPC/DMPG membrane (3:1) was used. Our recent ^{31}P NMR studies showed that TP interacts with POPC and POPC/POPG (3:1) mixtures in a very similar fashion; thus, the peptide structure is expected to be the same in the two membranes (*11*). The peptide/lipid solution was ultracentrifuged, and the wet pellet was used for the C−H REDOR experiments. The level of binding of the peptide to the lipid was ~90% based on UV−VIS absorption. For torsion angle measurements, ^{1}H spin diffusion, and ^{13}C−^{31}P REDOR experiments, the peptide/lipid solution was lyophilized and rehydrated to 35 wt % water. For the ^{13}C−^{31}P REDOR experiments, 20 wt % trehalose was added to the solution and the membrane mixture was lyophilized and directly used for the experiment. The replacement of water with trehalose, or lyoprotection, retains the lamellar structure of the membrane without the excessive lipid motions (*12*). The removal of lipid headgroup motion is necessary for measuring the distances between the lipid and the peptide.

NMR Experiments. All NMR experiments were carried out on a Bruker (Karlsruhe, Germany) DSX-400 spectrometer operating at a resonance frequency of 400.49 MHz for ^{1}H, 162.12 MHz for ^{31}P, 100.70 MHz for ^{13}C, and 40.58 MHz for ^{15}N. Triple-resonance MAS probes with a 4 mm spinning module were used. Low-temperature experiments were conducted using air cooled by a Kinetics Thermal Systems (Stone Ridge, NY) XR air-jet sample cooler. The typical cross polarization (CP) time was 0.7 ms, except for the ^{1}H−^{15}N Lee−Goldburg cross polarization (LG-CP) time in the C−H REDOR experiment, which was 100 μs to ensure that only the amide proton polarization is detected through ^{15}N. Typical radiofrequency (rf) fields were 50 kHz, except for ^{1}H dipolar decoupling during heteronuclear pulses and ^{1}H homonuclear decoupling, which used stronger rf fields of ~75 kHz. The signal averaging time for each experiment was typically 1−2 weeks. ^{13}C and ^{15}N chemical shifts were referenced externally to the α-Gly ^{13}CO signal at 176.49 ppm on the TMS scale and the *N*-acetylvaline ^{15}N signal at 122.0 ppm on the NH_3 scale.

Torsion Angle Measurements. The Val_6 ψ torsion angle was measured using the NCCN technique, which correlates the $^{15}N_i$−$^{13}C\alpha_i$ and $^{13}CO_i$−$^{15}N_{i+1}$ dipolar couplings to produce the relative orientation of the two bonds (*13*, *14*). ^{13}Cα−^{13}CO double-quantum coherence was excited by the SPC5 sequence (*15*), which evolved under the ^{13}C−^{15}N dipolar coupling, which was recoupled by a REDOR pulse train (*16*). For each REDOR mixing time, a reference spectrum (S_0) without the ^{15}N pulses and a dephased spectrum with the ^{15}N pulses were measured. The average of the S/S_0 values of the Cα and CO signals was plotted as a function of mixing time to yield a ψ angle-dependent curve. This was fit to yield the ψ angle. The samples were spun at 5−6 kHz for the NCCN experiment, and the pulse sequence was previously tested on the Gly-Ala-Leu tripeptide (*17*).

The ϕ torsion angle of Val_6 was measured using the HNCH technique, which correlates the $^{1}H^{N}$−^{15}N and $^{13}C\alpha$−$^{1}H\alpha$ dipolar couplings (*18*). ^{1}H homonuclear decoupling during the heteronuclear evolution was achieved using MREV-8. The measured H^{N}−N−Cα−Hα angle (ϕ_H) is related to the conventional ϕ angle according to the relation $\phi = \phi_H + 60°$. A slow spinning speed of 3.472 kHz was used to optimize the performance of MREV-8 homonuclear decoupling. The HNCH experiment was tested on the model amino acid *N*-acetylvaline (*18*). Both the NCCN and HNCH experiments were conducted at 233 K to eliminate undesired local motion.

The Gly_{10} ϕ angle was determined by a ^{13}CO−$^{1}H^{N}$ REDOR distance experiment, as the α-CH_2 group of Gly prohibits the use of the HNCH technique (*19*). As usual, two experiments were conducted for each mixing time, one without the ^{13}C π pulses (S_0) and the other with the ^{13}C pulses (S). The time-dependent S/S_0 determines the coupling strength. Incomplete dephasing due to π pulse imperfections was taken into account by a scaling factor of 0.9 for the simulated REDOR curves. The Gly_{10} REDOR data were recorded at 238 K with 3.472 kHz MAS.

Distance Measurements. The Val_6 ^{13}CO−Phe_8 $^{1}H^{N}$ distance was measured using the ^{15}N-detected ^{13}C−^{1}H REDOR experiment (*20*). ^{1}H homonuclear decoupling during the REDOR mixing period was achieved using the MREV-8 sequence, with 90° pulse lengths ~3.5 μs in duration and synchronized with a MAS spinning speed of 3472 Hz. The experiment was recently conducted with the model compound ^{15}N- and ^{13}CO-labeled N-tBoc-glycine and yielded two distances (3.09 and 2.78 Å) that are consistent with the crystal structure (*19*). To account for dephasing of the H^{N} signal by natural abundance ^{13}C sites, we also measured the REDOR dephasing on a control TP sample with Phe_8 labeled with ^{15}N but no ^{13}C labeling. This ^{13}C natural abundance (n.a.) sample gave an S/S_0 plateau of ~0.93. The REDOR dephasing of only the ^{13}C label was then calculated with the relation $(S/S_0)_{label} = [(S/S_0)_{total} - (S/S_0)_{n.a.} + 0.93]/0.93$. The experiment was conducted at 233 K to ensure the dipolar couplings are in the rigid limit.

The lipid ^{31}P−peptide ^{13}CO distances were measured using ^{13}C−^{31}P REDOR. A single ^{13}C π pulse and multiple ^{31}P π pulses were applied. The dephasing of the natural abundance lipid ^{13}CO was measured with a control experiment on unlabeled TP. The ^{13}C−^{31}P REDOR simulations are the weighted average of the curves of the labeled and the unlabeled peptide, $(S/S_0)_{total} = 0.68(S/S_0)_{label} + 0.32(S/S_0)_{n.a.}$, where the weight fractions are calculated on the basis of the peptide:lipid molar ratio. The experiment was carried out at 253 K with 5 kHz MAS.

Qualitative information about the depth of insertion of TP was obtained from a two-dimensional (2D) ^{1}H spin diffusion experiment where spin diffusion from lipid and water protons to the peptide is detected through the peptide ^{13}C signals (*21*). The spin diffusion mixing times varied from 0.1 to 400 ms. A ^{1}H T_2 filter of 2 ms prior to the ^{1}H evolution period was used to destroy the ^{1}H magnetization of the rigid peptide while those of the mobile lipids and water were retained; 110 t_1 points were collected in the indirect ^{1}H dimension. The experiments were conducted at 299 K under 4 kHz MAS.

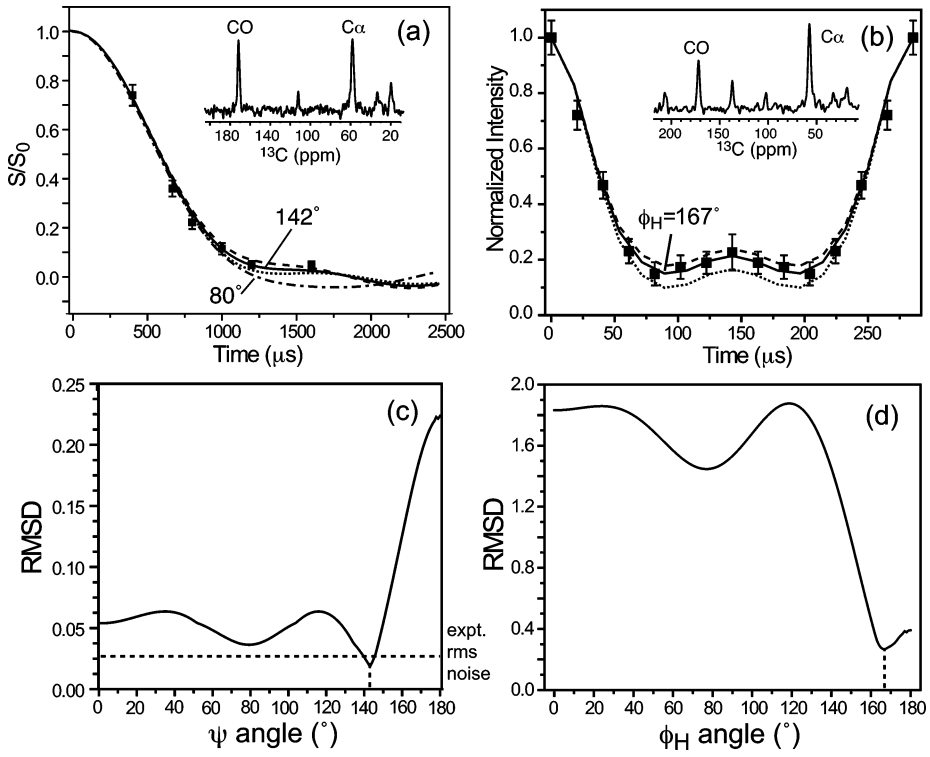

FIGURE 1: ϕ and ψ torsion angles of Val$_6$ of TP in DMPC bilayers at 233 K. (a) NCCN data for ψ angle determination. A representative spectrum, with an N−C mixing time of 667 μs, is shown. The best fit is obtained with a ψ of ±142° (—), flanked by the curves for values of ±144° (- - -) and ±140° (•••). The simulated curve for a ψ of ±80° (− - −) is also shown and deviates from the data at long times. (b) HNCH data for ϕ angle determination. A representative spectrum is shown. The best fit is obtained with a ϕ_H of ±167° (—), flanked by the curves for values of ±177° (- - -) and ±157° (•••). rmsd plots comparing the experiment with the simulations for the NCCN (c) and HNCH (d) data quantitatively indicate the best-fit torsion angles.

RESULTS

Secondary Structure of TP in DMPC Bilayers. To constrain the secondary structure of TP in lipid bilayers, we measured the ϕ and ψ torsion angles of Val$_6$. Laederach et al. (*8*) found this residue to be the hinge of a bent conformation in 320 mM DPC micelles, while Kawano and co-workers (*9*) found the peptide to have straight β-strands in 60 mM DPC micelles. We measured the Val$_6$ ϕ and ψ angles directly in DMPC bilayers by correlating the dipolar couplings along the two bonds flanking the torsion bond of interest. For the ϕ angle, this involves the N−H and Cα−Hα dipolar couplings (*18*), while for the ψ angle, the N−Cα and C′−N dipolar couplings are correlated (*13*). Figure 1 shows the NCCN (a) and HNCH (b) curves of TP with uniformly ^{13}C- and ^{15}N-labeled Val$_6$ and ^{15}N-labeled Cys$_7$. The NCCN data are best fit with a $|\psi|$ of 142 ± 2°, while the HNCH data give a $|\phi_H|$ of 167 ± 10°, as shown by the rmsd analysis (Figure 1c,d). Since $\phi = \phi_H + 60°$, the ϕ angle is −133 ± 10° or −107 ± 10°. Combined, the two torsion angles indicate that Val$_6$ adopts a canonical antiparallel β-sheet conformation. Each experiment gives two degenerate angles due to the uniaxial nature of the dipolar coupling tensor. However, the negative ψ angle can be ruled out since it occurs in an unpopulated region of the Ramachandran diagram for Val residues. For the ϕ angle results, the −107° value is closer to that of the parallel β-sheet conformation. However, typical parallel β-sheets have a ψ angle of ∼110°, which is ruled out by the NCCN data.

Figure 2 shows the $\phi-\psi$ Ramachandran diagram of Val$_6$ where the solid-state NMR results (○) are compared with

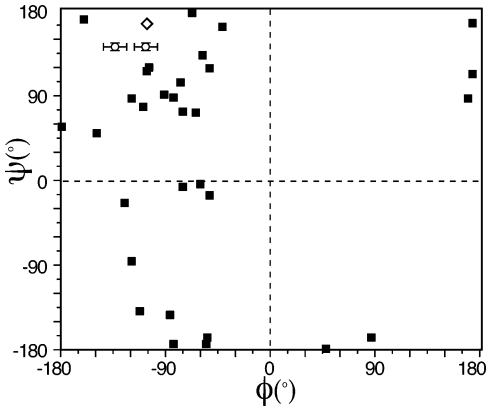

FIGURE 2: Ramachandran diagram of TP Val$_6$ in DMPC bilayers measured by solid-state NMR (○). For comparison, the ensemble of 30 solution NMR structures of TP in a 320 mM DPC micelle solution (■) and the single structure in a 60 mM DPC micelle solution (◇) are shown.

the two solution NMR results. The high-concentration DPC micelle data, which are an ensemble of 30 structures (squares), exhibit a significant conformational distribution. In comparison, the conformation in DMPC bilayers obtained from solid-state NMR clearly falls into the β-sheet region of the diagram with a relatively small angular distribution. The ordered nature of the peptide conformation is also reflected in the ^{13}C line widths of Val$_6$ and Gly$_{10}$, which are ∼2.8 ppm. This conformational homogeneity is similar to the low-concentration DPC micelle result (◇).

^{13}C isotropic chemical shifts of Val$_6$ support the torsion angle results. The CO and Cα shifts are 171.9 and 57.6 ppm, respectively. These differ from the random coil values by

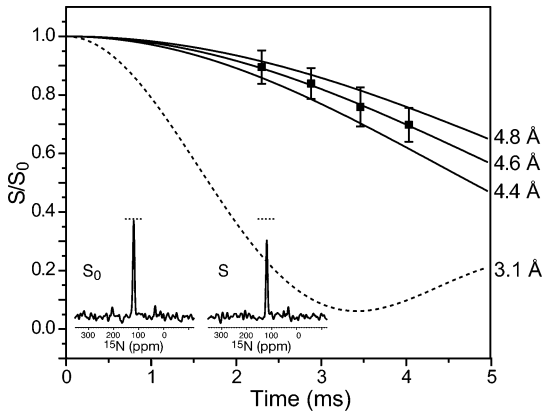

FIGURE 3: ^{15}N-detected Val$_6$ ^{13}CO−Phe$_8$ ^{1}H^{N} REDOR data of TP in a DMPC/DMPG membrane. Representative ^{15}N S_0 and S spectra are shown for a mixing time of 2.88 ms. The S/S_0 values had been corrected for dipolar dephasing by natural abundance ^{13}CO sites. The best fit is obtained at a distance of 4.6 ± 0.2 Å. The 3.1 Å curve (- - -) predicted from the high-concentration DPC micelle structure is shown for comparison. Simulated curves were scaled by 0.9 to account for incomplete dephasing due to pulse imperfections (*34*).

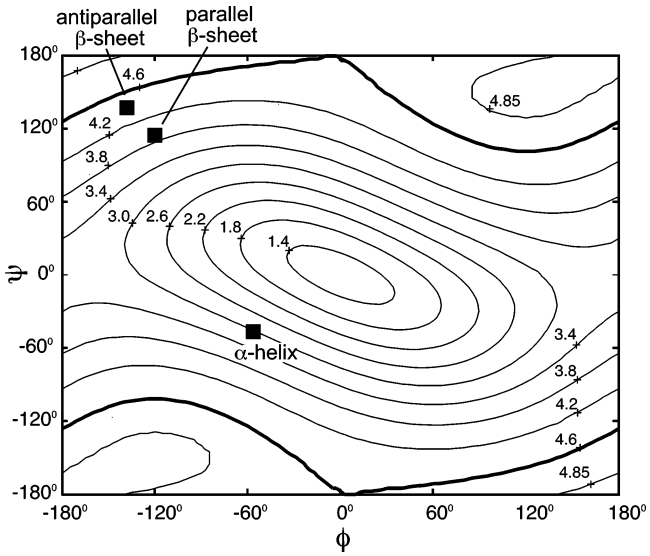

FIGURE 4: Val$_6$ CO−Phe$_8$ H^{N} distance as a function of Cys$_7$ ϕ and ψ angles. A peptide bond torsion angle of 180° and standard bond angles and bond lengths were used. The 4.6 Å distance contour is shown as a thick line. The positions of the standard β-sheet and α-helical conformations are indicated for comparison.

−2.1 and −2.8 ppm, respectively, indicating a well-defined β-sheet structure (*22*).

To further constrain the conformation of TP in the central part of the N-terminal strand, we measured the distance between Val$_6$ CO and Phe$_8$ H^{N}. This distance spans five covalent bonds and thus depends on the torsion angles of the central three bonds, N$_7$−Cα$_7$, Cα$_7$−CO$_7$, and CO$_7$−N$_8$. The CO$_7$−N$_8$ peptide bond has a known torsion angle of 180°. Thus, the Val$_6$ CO−Phe$_8$ H^{N} distance is mainly determined by the ϕ and ψ angles of Cys$_7$. The CO−H^{N} REDOR data are shown in Figure 3. S/S_0 decays to 0.72 by 4.03 ms. The data have been corrected for dephasing by natural abundance ^{13}CO sites in the lipid and the peptide through a control experiment on TP not labeled with ^{13}C but labeled with ^{15}N at Phe$_8$ in a DMPC membrane. The corrected data are best fit by a C−H distance of 4.6 ± 0.2 Å. To convert this distance to Cys$_7$ ϕ and ψ torsion angles, we display the CO$_6$−H$^{N}_8$ distance as a function of ϕ and ψ angles in Figure 4. The 4.6 Å distance (thick lines) is near the maximum physically allowed distance of 4.9 Å between the two atoms and is satisfied by relatively large ψ angle values. Excluding negative ϕ and ψ angles, which are outside the allowed regions of the conformational space for this non-Gly residue, we find that the Cys$_7$ torsion angles are closest to the antiparallel β-sheet structure, consistent with the direct Val$_6$ torsion angle measurement results.

TP contains two disulfide bonds, Cys$_7$−Cys$_{12}$ and Cys$_3$−Cys$_{16}$. These impose strong constraints on the conformation of residues 8−12. Solution NMR data show these residues to form a β-turn in both water and micelles (*8*). However, the β-turn nature of these residues in lipid bilayers has not been directly verified. Thus, we measured the Gly$_{10}$ ϕ torsion angle. Since Gly has two Hα protons, the HNCH experiment cannot be used. Instead, we measured the intraresidue three-bond CO−H^{N} distance, which is determined only by the torsion angle of the central N−Cα bond, i.e., the ϕ angle. Figure 5a shows the CO−H^{N} REDOR data of Gly$_{10}$ ^{13}CO- and ^{15}N-labeled TP in DMPC bilayers. In contrast to the Val$_6$−Phe$_8$ C−H REDOR data, the Gly$_{10}$ dephasing was rapid, reaching a low S/S_0 value of ∼0.2 by 2.3 ms. The simulation yielded a distance of 3.05 ± 0.10 Å. Figure 5b shows the ϕ angle dependence of the CO−H^{N} distance. The 3.05 Å distance corresponds to a ϕ angle of ±85°, and the angular uncertainty from the distance measurement is ±15°. The ϕ angle of ±85° is distinct from that of the standard α-helix and β-sheet conformations but corresponds to a β-turn conformation. Since Gly$_{10}$ is at the putative $i + 2$ position of the turn, this value is consistent with a type I, I′, II, II′, V, or V′ β-turn (*23*).

Membrane Binding Topology. To quantitatively determine the depth of insertion of TP in lipid bilayers, we carried out a ^{13}C−^{31}P REDOR experiment between ^{13}CO-labeled TP and the lipid ^{31}P in DMPC/DMPG (3:1) bilayers. To ensure that the lipid motion is frozen, we used trehalose-cryoprotected dry lipid membranes. The ^{13}C−^{31}P REDOR curves for Val$_6$ ^{13}CO and Gly$_{10}$ ^{13}CO groups after natural abundance correction are shown in Figure 6. The two labels show very similar S/S_0 values, both of which are best fit to a ^{13}C−^{31}P distance of 6.8 ± 0.4 Å. For simplicity, only two-spin simulations are used here to fit the distance data, since the main conclusion of interest is the relative distance from Val$_6$ and Gly$_{10}$ to the phosphate groups. Multispin simulations (*24*) incorporating, for example, three ^{31}P atoms do not increase the vertical distance between the ^{31}P plane and the ^{13}C label, even though they yield individual ^{13}C−^{31}P distances that are ∼1.0 Å longer than that of the two-spin simulation. Thus, the depths of insertion of the Val$_6$ and Gly$_{10}$ residues from the membrane plane are similar and both 6−7 Å.

Complementing the ^{13}C−^{31}P experiment, a 2D ^{1}H spin diffusion experiment was used to measure the proximity of the peptide to the lipid chains in the center of the membrane. Figure 7 shows two 2D ^{13}C-detected ^{1}H spin diffusion spectra, acquired with a mixing time of 0.1 (a) or 100 ms (b). No lipid ^{1}H−peptide ^{13}C cross-peaks are observed at 0.1 ms, while clear cross-peaks between the water protons (4.6 ppm) and Val$_6$ Cγ (19.6 ppm) and between the lipid CH$_2$ protons (1.3 ppm) and Val$_6$ Cγ are detected at 100 ms.

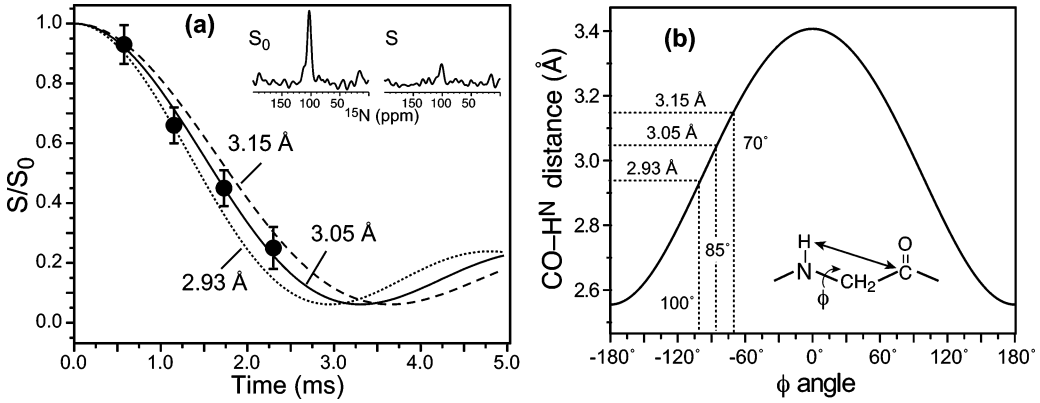

FIGURE 5: TP Gly$_{10}$ ϕ angle determination by CO−H^N REDOR. (a) Intraresidue ^{13}CO−^{1}H^N REDOR curve. The best fit is obtained with a distance of 3.05 Å [506 Hz (—)]. Simulated curves for 3.15 Å [458 Hz (- - -)] and 2.93 Å [566 Hz (···)] are shown to indicate the uncertainty. The C−H couplings have been scaled by the MREV-8 scaling factor of 0.47. Simulated curves are scaled by 0.9 from the ideal REDOR curve to account for incomplete dephasing due to pulse imperfections. Representative S_0 and S spectra are shown for a mixing time of 2.3 ms. (b) Curve relating the CO−H^N distance to the ϕ torsion angle. For distances of 2.93, 3.05, and 3.15 Å, the ϕ angles are ±100°, ±85°, and ±70°, respectively.

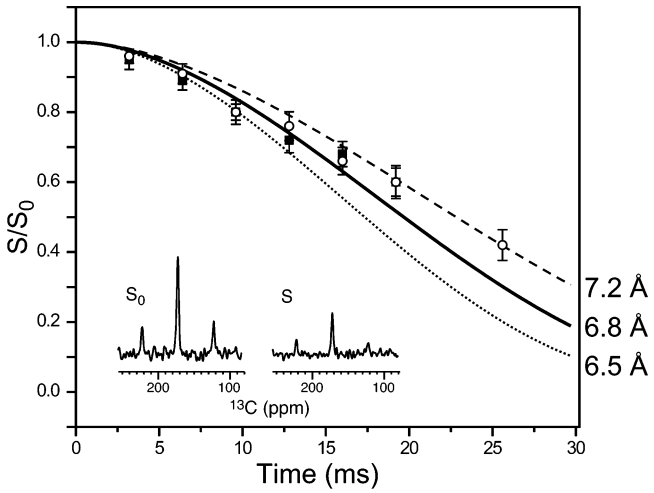

FIGURE 6: ^{13}C−^{31}P REDOR data of TP in a DMPC/DMPG/trehalose membrane. The Val$_6$ ^{13}CO (○) and Gly$_{10}$ ^{13}CO (■) data are shown. The best fit for both is obtained at a ^{13}C−^{31}P distance of 6.8 Å [39 Hz (—)] using a two-spin simulation. Simulated curves for 7.2 Å [33 Hz (- - -)] and 6.5 Å [45 Hz (···)] are also shown to indicate the distance uncertainty. Representative S_0 and S spectra are shown for a mixing time of 25.6 ms for the Val$_6$ data.

The lack of cross-peaks at 0.1 ms is an important control proving that the magnetization of the mobile Val methyl protons directly bonded to the detected Cγ is suppressed by the ^{1}H T_2 filter. Thus, the 1.3 ppm cross-peak at longer mixing times must originate from the mobile lipid chain protons. Previous experiments on DNA intercalated with multilamellar lipid membranes indicate that when a macromolecule is bound to the membrane surface, ∼20 Å from the hydrophobic center, it exhibits virtually no cross-peaks with the lipid chain protons after 100 ms. Thus, the presence of a clear lipid CH_2 cross-peak with TP qualitatively indicates that the peptide is immersed in the membrane, below the ^{31}P-rich membrane surface. The Val$_6$ Cγ ^{1}H cross sections for a number of mixing times are shown in Figure 7c. The T_1-corrected CH_2 intensities show a monotonic increase without a plateau being reached by 400 ms (not shown). This differs from the case for transmembrane proteins such as colicin Ia channel domain (*21*) or protegrin-1 (*25*), whose CH_2 and CH_3 cross-peaks reach a plateau by ∼100 ms. Thus, the depth of insertion of TP is intermediate between completely surface bound molecules and fully membrane spanning molecules. Extraction of more quantitative distances from the cross-peak intensity buildup is difficult because the TP backbone is mobile in the liquid-crystalline phase of the membrane at this temperature, as evidenced by the lack of the Val$_6$ backbone ^{13}C signals in the spectra (not shown). This peptide mobility reduces the diffusion coefficient contrast between the lipid and the peptide, which is necessary for the distance quantification (*21*).

DISCUSSION

The data given above indicate that the N-strand of TP adopts an ideal antiparallel β-sheet conformation in DMPC bilayers. The Val$_6$ residue has ϕ and ψ torsion angles of −133° and 142°, respectively. The Val$_6$ ^{13}CO−Phe$_8$ H^N distance is 4.6 ± 0.2 Å, which is satisfied by an antiparallel β-sheet conformation for Cys$_7$. At Gly$_{10}$, a nonsheet ϕ angle of 85 ± 15° was measured, which is consistent with the i + 2 residue of a type I, I′, II, II′, V, or V′ β-turn conformation. This confirms that the two disulfide bonds indeed constrain the overall peptide fold to a β-hairpin in lipid membranes. For comparison, the solution NMR results for the Gly$_{10}$ ϕ angle are −154° in low-concentration DPC micelles and 114 ± 55° in high-concentration DPC micelles (*8*, *9*).

Figure 8a shows the DMPC-bound TP structure obtained by solid-state NMR. The structure is derived from the low-concentration DPC structure (Figure 8b) (*9*) by making small changes in the Val$_6$, Cys$_7$, and Gly$_{10}$ ϕ and ψ angles to satisfy the distance and torsion angle constraints obtained here. When the Gly$_{10}$ ϕ angle was changed to 80°, the other torsion angles of Arg$_9$ and Gly$_{10}$ also needed to be modified to retain the β-hairpin motif. Molecular modeling shows that, when only standard β-turn torsion angles are used, then among the six possible β-turns consistent with the Gly$_{10}$ data, only the type II β-turn gives a relatively ideal hairpin with collinear strands. This is the structure shown in Figure 8a. For comparison, Figure 8c shows a typical TP structure in high-concentration DPC micelles, with a pronounced curvature in the two strands around Arg$_5$ and Arg$_{14}$ (*8*). As a result, the high-concentration micelle structure has an average Val$_6$ CO−Phe$_8$ H^N distance of 3.1 Å, much shorter than the distance of 4.6 Å measured in DMPC/DMPG bilayers.

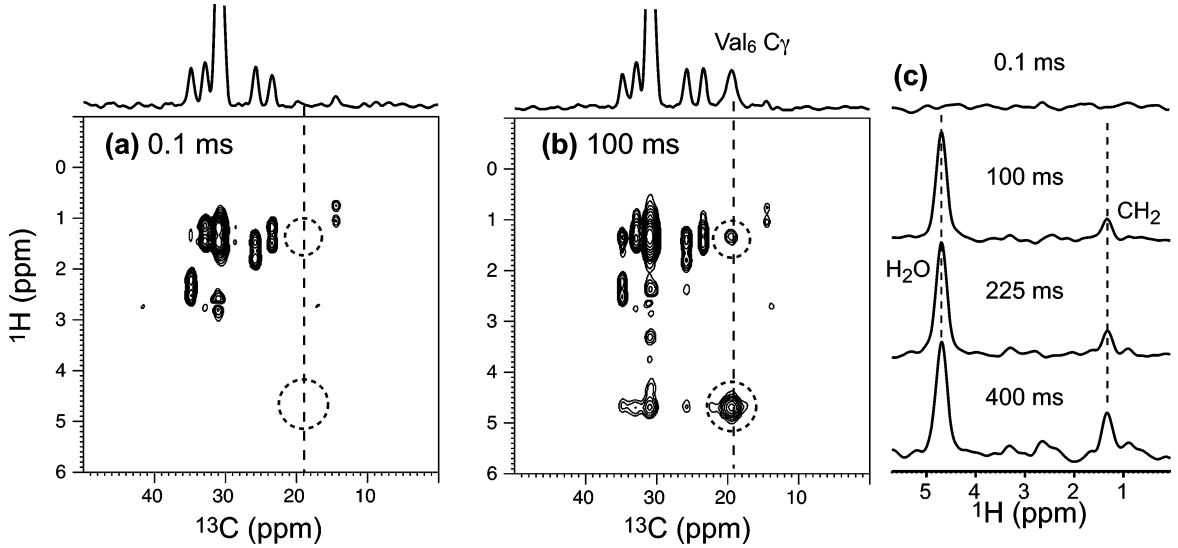

FIGURE 7: ^{13}C-detected ^{1}H spin diffusion spectra of TP uniformly ^{13}C- and ^{15}N-labeled at Val_6 in DMPC membranes at 299 K (*2*). 2D spectrum after a mixing time of 0.1 ms. No Val_6 Cγ peaks are observed. (b) 2D spectrum at a mixing time of 100 ms. Val_6 Cγ cross-peaks with water and lipid CH_2 protons are detected (dashed circles). The ^{13}C projection is shown above each 2D spectrum. Note the absence of the Val Cγ signal at 0.1 ms. (c) Val_6 Cγ ^{1}H cross sections for various spin diffusion mixing times.

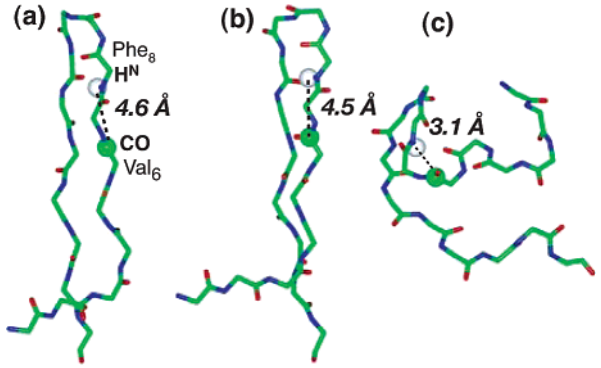

FIGURE 8: Conformation of TP in (a) DMPC bilayers as determined by solid-state NMR, (b) a 60 mM DPC micelle solution (*9*), and (c) a 320 mM DPC micelle solution (*8*). The Val_6 CO−Phe_8 H^N distance differs in the three structures. The type of β-turn also differs between the bilayer-bound structure and the micelle-bound structures. The molecules were visualized in Insight II.

Induction of peptide curvature by detergent micelles has been observed before. For example, HIV-1 envelope protein gp41 shows a bent α-helical structure in DHPC micelles but becomes a straight helix in bicelles aligned in a stretched polyacrylamide gel (*26*). Such curvature is usually attributed to the small size of the micelles compared to lipid bilayers or bicelles. However, this curvature argument seems inadequate for explaining the different TP structures in the 60 and 320 mM DPC micelle solutions, since both concentrations are above the critical micelle concentration of DPC. In fact, at higher concentrations, larger micelles would be expected, which should cause less peptide curvature. The main experimental constraints for the bent structure are long-range ^{1}H NOE cross-peaks between Trp_2 and Arg_9, Phe_4 and Val_6, and Tyr_{13} and Arg_{15} (*8*). We speculate that these cross-peaks could originate from intermolecular, rather than intramolecular, contacts, as a result of peptide oligomerization in the high-DPC concentration sample.

The most intriguing aspects of the TP structure are its depth of insertion and potential orientation. If the peptide fully spans the membrane, perpendicular to the membrane plane, then one would expect Val_6 in the middle of the N-terminal strand to be located in the hydrophobic part of the membrane, far from the lipid headgroups, while Gly_{10} at the β-turn would be much closer to the headgroups. However, the $^{13}C-^{31}P$ distance measurements showed that Val_6 and Gly_{10} carbonyl carbons are equidistant, 6.8 ± 0.4 Å, from the ^{31}P atoms of the DMPC/DMPG membrane. This strongly suggests that the β-hairpin is approximately parallel to the membrane surface (Figure 9a). Moreover, since the ^{1}H spin diffusion experiments indicate that the Val_6 Hγ protons receive magnetization from the lipid CH_2 protons in 100 ms, which is fast compared to membrane surface-bound molecules such as DNA (*21*), Val_6 must be immersed below the membrane surface, not far from the top of the acyl chains. Thus, combining the distance constraints to ^{31}P and to the lipid CH_2 protons, we conclude TP is most likely immersed in the glycerol backbone and lipid carboxyl region. In fact, the peptide−lipid $^{13}C-^{31}P$ distance is very similar to the intramolecular lipid $^{13}CO-^{31}P$ distance, further supporting this conclusion.

Figure 9a shows the solid-state NMR-refined TP structure in a planar orientation, superimposed with a schematic representation of liquid-crystalline DMPC bilayers. The thickness of the bilayer is obtained from a MD simulation (*27*) and is drawn to scale with TP. Immersed in the membrane, each β-hairpin would have nine unsatisfied hydrogen bonds exposed to the interfacial region of the bilayer. White and co-workers (*28*) estimated an energy penalty of 0.5 kcal/mol for the transfer of an unsatisfied hydrogen bond from the aqueous solution to the membrane interface. However, this energy cost is likely balanced by the favorable insertion of the hydrophobic side chains of Trp_2, Phe_4, Tyr_8, and Try_{13} in TP. It is also possible that TP is oligomerized in the lipid membrane, as we found for the analogous peptide PG-1 (*29*, *30*), which would reduce the number of unsatisfied hydrogen bonds per molecule.

The current data do not rule out an alternative scenario where TP may be partially inserted into the lipid bilayer in a transmembrane orientation, with Gly_{10} CO outside the membrane surface and Val_6 CO below the membrane surface,

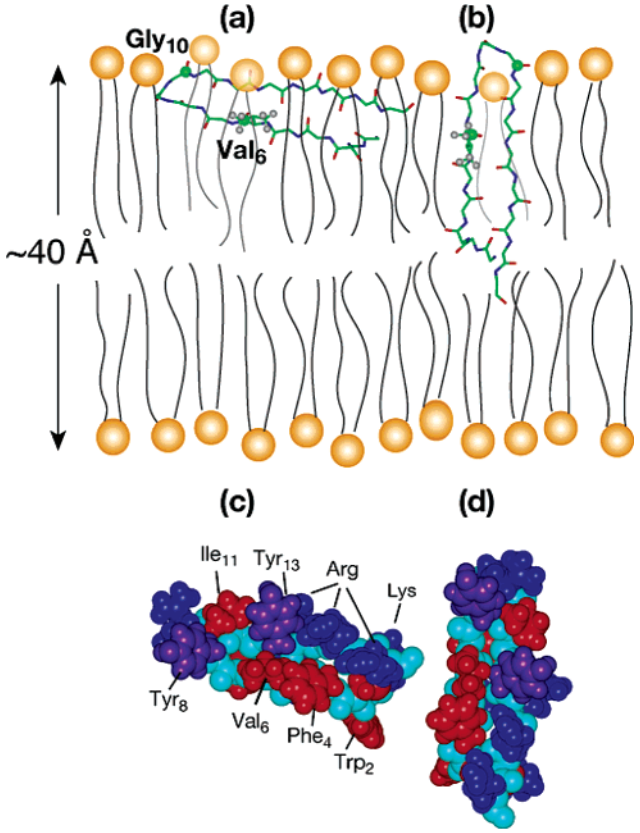

FIGURE 9: Models of binding of TP to DMPC bilayers. TP and DMPC bilayer thicknesses are drawn to scale. (a) TP is immersed in the glycerol backbone region in a horizontal fashion. (b) TP is oriented normal to the membrane plane and partially inserted. (c and d) Side chain hydrophobicities of TP in the two orientations. Red denotes hydrophobic residues (Val, Phe, Trp, Ile, and Cys), blue hydrophilic residues (Arg and Lys), and purple Tyr.

equidistant from the ^{31}P atoms (Figure 9b). In this way, the Val_6 side chain can still be in spin diffusion contact with the lipid CH_2 protons. However, this transmembrane orientation is less likely than the planar orientation for several reasons. First, the peptide is not long enough to span the DMPC bilayer in a transmembrane fashion, especially if the Gly_{10}-containing β-turn is outside the membrane surface (Figure 9b). Second, polar residues such as Arg_5, Arg_{14}, and Arg_{15} would be embedded in the hydrophobic region of the membrane, which is energetically costly. Third, the distribution of the polar and nonpolar residues in TP makes a transmembrane orientation and insertion unfavorable. Panels c and d of Figure 9 show the side chain hydrophobicity of TP in these two orientations. A mostly hydrophobic face is present in the peptide, consisting of Trp_2, Phe_4, Val_6, Cys_7, and Tyr_8 side chains. The other face mainly consists of the polar Arg and Lys residues. The horizontal orientation places the hydrophobic face toward the hydrophobic interior of the membrane and the cationic face toward the polar exterior. In contrast, the transmembrane orientation makes this amphiphilic interface of the peptide perpendicular to that of the membrane, which is unfavorable.

The interpretations given above of the depth of insertion of TP assume that the lipid bilayer maintains its lamellar structure in the presence of TP, without any defects that would destroy the planarity of the membrane surface where the ^{31}P atoms are. This assumption is valid for the DMPC and DMPC/DMPG membranes used here. Our recent glass-

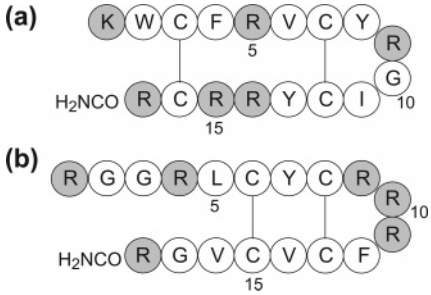

FIGURE 10: Amino acid sequence of (a) TP and (b) PG-1.

plate oriented ^{31}P spectra for TP-including membranes showed that the peptide does not perturb the orientational order of neutral POPC bilayers or POPC/POPG membranes but create isotropic vesicles in POPE/POPG lipid mixtures (*11*). Direct ^{31}P powder spectra (not shown) of the MAS samples used here also confirm the lack of any isotropic peaks. Thus, there is no detectable pore structure in the membrane under the experimental conditions described here.

The conclusion that TP is parallel to the membrane plane and immersed in the interfacial region of the membrane is in good qualitative agreement with polarized attenuated total reflection Fourier transform infrared (ATR-FTIR) data (*6*): the dichroic ratio of the amide I′ band is consistent with the β-sheet lying parallel to the plane of the membrane, while the lipid CH_2 symmetric stretching band indicates that the order parameter of the acyl chains is slightly reduced by TP, indicating that the peptide penetrates slightly into the hydrophobic region of the membrane. In addition, Trp fluorescence data indicated that Trp_2 of TP is located in the hydrophobic environment near the surface of the lipid membrane (*4*).

A related study on a cysteine-deleted version of TP (CDT) was recently carried out. On the basis of the effect of CDT on the phase transition of the lipids observed through DSC, the authors suggested that the peptide is located at the membrane interface without being inserted into the hydrophobic part of the membrane (*31*). If confirmed by direct orientation measurements, this would suggest that an in-plane orientation may be a common feature of the TP family of peptides as a result of its distribution of hydrophobic and hydrophilic residues and independent of the disulfide bonds. A similar in-plane orientation was also suggested for the hydrophilic disulfide-bridged β-sheet peptide androctonin, based on the dichroic ratios of the lipid chain CH_2 stretching bands in the polarized ATR-FTIR spectra (*32*). However, androctonin was thought to be lying on the surface of the membrane rather than in the interfacial region, since the lipid order parameter did not change upon peptide binding.

Interestingly, the proposed membrane insertion and orientation of TP are quite different from those of protegrin-1 (PG-1), a similar disulfide-stabilized β-hairpin antimicrobial peptide. ^{1}H spin diffusion and paramagnetic dephasing experiments clearly indicated that PG-1 completely spans the lipid membrane (*25*, *33*). Direct orientation measurement indicated that the β-strand axis of PG-1 is tilted by ~55° from the membrane normal in DLPC bilayers (*10*). When the amino acid sequences of the two peptides are compared (Figure 10), the main difference is that TP has two cationic Arg residues in the middle of the C-terminal strand while the middle of the PG-1 C-terminal strand is

completely hydrophobic. The remaining charges are distributed in similar positions of the two peptides. Thus, it appears that small changes in charge distribution can significantly affect the membrane-bound structure of these antimicrobial peptides, and consequently their mechanisms of action.

In conclusion, we find that TP adopts an antiparallel β-sheet conformation in lipid bilayers with a β-turn at Gly_{10} connecting the two strands. No bending is present in the middle of the two strands. The peptide is immersed in the glycerol backbone region of the membrane, with Val_6 and Gly_{10} CO groups equidistant from the lipid ^{31}P, and with the Val_6 side chain in close spin diffusion contact with the lipid acyl chain CH_2 protons. These suggest a planar orientation of the peptide in DMPC and DMPC/DMPG bilayers. Further experiments involving direct orientational determination are necessary to definitively determine the membrane binding topology of TP.

REFERENCES

1. Nakamura, T., Furunaka, H. T. T. M., Tokunaga, F., Muta, T., Iwanaga, S., Niwa, M., Takao, T., and Shimonishi, Y. (1988) Tachyplesin, a class of antimicrobial peptide from the hemocytes of the horseshoe crab (*Tachypleus tridentatus*). Isolation and chemical structure, *J. Biol. Chem. 263*, 16709−16713.
2. Rao, A. G. (1999) Conformation and antimicrobial activity of linear derivatives of tachyplesin lacking disulfide bonds, *Arch. Biochem. Biophys. 361*, 127−134.
3. Matsuzaki, K. (1999) Why and how are peptide-lipid interactions utilized for self-defense? Magainins and tachyplesins as archetypes, *Biochim. Biophys. Acta 1462*, 1−10.
4. Matsuzaki, K., Fukui, M., Fujii, N., and Miyajima, K. (1991) Interactions of an antimicrobial peptide, tachyplesin I, with lipid membranes, *Biochim. Biophys. Acta 1070*, 259−264.
5. Matsuzaki, K., Yoneyama, S., Fujii, N., Miyajima, K., Yamada, K., Kirino, Y., and Anzai, K. (1997) Membrane permeabilization mechanisms of a cyclic antimicrobial peptide, tachyplesin I, and its linear analog, *Biochemistry 36*, 9799−9806.
6. Matsuzaki, K., Nakayama, M., Fukui, M., Otaka, A., Funakoshi, S., Fujii, N., Bessho, K., and Miyajima, K. (1993) Role of disulfide linkages in tachyplesin-lipid interactions, *Biochemistry 32*, 11704−11710.
7. Kawano, K., Yoneya, T., Miyata, T., Yoshikawa, K., Tokunaga, F., Terada, Y., and Iwanaga, S. (1990) Antimicrobial peptide, tachyplesin I, isolated from hemocytes of the horseshoe crab (*Tachypleus tridentatus*). NMR determination of the β-sheet structure, *J. Biol. Chem. 265*, 15365−15367.
8. Laederach, A., Andreotti, A. H., and Fulton, D. B. (2002) Solution and micelle-bound structures of tachyplesin I and its active aromatic linear derivatives, *Biochemistry 41*, 12359−12368.
9. Mizuguchi, M., Kamata, S., Kawabata, S., Fujitani, N., and Kawano, K. (2005) in *Protein Data Bank*, RCSB Protein Data Bank.
10. Yamaguchi, S., Waring, A., Hong, T., Lehrer, R., and Hong, M. (2002) Solid-State NMR Investigations of Peptide-Lipid Interaction and Orientation of a β-Sheet Antimicrobial Peptide, Protegrin, *Biochemistry 41*, 9852−9862.
11. Doherty, T., Waring, A. J., and Hong, M. (2006) Peptide-lipid interactions of the β-hairpin antimicrobial peptide tachyplesin and its linear derivatives from solid-state NMR, *Biochim. Biophys. Acta 1758*, 1285−1291.
12. Crowe, J. H., Crowe, L. M., and Chapman, D. (1984) Preservation of Membranes in Anhydrobiotic Organisms: The Role of Trehalose, *Science 223*, 701−703.
13. Costa, P. R., Gross, J. D., Hong, M., and Griffin, R. G. (1997) Solid-State NMR Measurement of ψ in Peptides: A NCCN 2Q-Heteronuclear Local Field Experiment, *Chem. Phys. Lett. 280*, 95−103.
14. Feng, X., Eden, M., Brinkmann, A., Luthman, H., Eriksson, L., Graslund, A., Antzutkin, O. N., and Levitt, M. H. (1997) Direct determination of a peptide torsion angle ψ by double-quantum solid-state NMR, *J. Am. Chem. Soc. 119*, 12006−12007.
15. Hohwy, M., Rienstra, C. M., Jaroniec, C. P., and Griffin, R. G. (1999) Fivefold symmetric homonuclear dipolar recoupling in rotating solids: Application to double-quantum spectroscopy, *J. Chem. Phys. 110*, 7983−7992.
16. Gullion, T., and Schaefer, J. (1989) Rotational echo double resonance NMR, *J. Magn. Reson. 81*, 196−200.
17. Yao, X. L., and Hong, M. (2004) Structural Distribution in an Elastin-Mimetic Peptide $(VPGVG)_3$ Investigated by Solid-State NMR, *J. Am. Chem. Soc. 126*, 4199−4210.
18. Hong, M., Gross, J. D., and Griffin, R. G. (1997) Site-resolved determination of peptide torsion angle ϕ from the relative orientations of backbone N-H and C-H bonds by solid-state NMR, *J. Phys. Chem. B 101*, 5869−5874.
19. Sinha, N., and Hong, M. (2003) X-^{1}H rotational-echo double-resonance NMR for torsion angle determination of peptides, *Chem. Phys. Lett. 380*, 742−748.
20. Schmidt-Rohr, K., and Hong, M. (2003) Measurements of carbon to amide-proton distances by C-H dipolar recoupling with ^{15}N NMR detection, *J. Am. Chem. Soc. 125*, 5648−5649.
21. Huster, D., Yao, X. L., and Hong, M. (2002) Membrane Protein Topology Probed by ^1H Spin Diffusion from Lipids Using Solid-State NMR Spectroscopy, *J. Am. Chem. Soc. 124*, 874−883.
22. Zhang, H., Neal, S., and Wishart, D. S. (2003) RefDB: A database of uniformly referenced protein chemical shifts, *J. Biomol. NMR 25*, 173−195.
23. Creighton, T. E. (1993) *Proteins: Structures and molecular properties*, 2nd ed., W. H. Freeman and Co., New York.
24. Tang, M., Waring, A., and Hong, M. (2006) *J. Magn. Reson.*, submitted.
25. Buffy, J. J., Waring, A. J., Lehrer, R. I., and Hong, M. (2003) Immobilization and Aggregation of Antimicrobial Peptide Protegrin in Lipid Bilayers Investigated by Solid-State NMR, *Biochemistry 42*, 13725−13734.
26. Chou, J. J., Kaufman, J. D., Stahl, S. J., Wingfield, P. T., and Bax, A. (2002) Micelle-induced curvature in a water-insoluble HIV-1 Env peptide revealed by NMR dipolar coupling measurement in stretched polyacrylamide gel, *J. Am. Chem. Soc. 124*, 2450−2451.
27. de Groot, B. L., Tieleman, D. P., Pohl, P., and Grubmuller, H. (2002) Water permeation through gramicidin A: Desformylation and the double helix: A molecular dynamics study, *Biophys. J. 82*, 2934−2942.
28. White, S. H., and Wimley, W. C. (1999) Membrane Protein Folding and Stability: Physical Principles, *Annu. Rev. Biophys. Biomol. Struct. 28*, 319−365.
29. Buffy, J. J., Waring, A. J., and Hong, M. (2005) Determination of Peptide Oligomerization in Lipid Membranes with Magic-Angle Spinning Spin Diffusion NMR, *J. Am. Chem. Soc. 127*, 4477−4483.
30. Mani, R., Tang, M., Wu, X., Buffy, J. J., Waring, A. J., Sherman, M. A., and Hong, M. (2006) Membrane-bound dimer structure of a β-hairpin antimicrobial peptide from rotational-echo double-resonance solid-state NMR, *Biochemistry 45*, 8341−8349.
31. Ramamoorthy, A., Thennarasu, S., Tan, A., Gottipati, K., Sreekumar, S., Heyl, D. L., An, F. Y., and Shelburne, C. E. (2006) Deletion of all cysteines in tachyplesin I abolishes hemolytic activity and retains antimicrobial activity and lipopolysaccharide selective binding, *Biochemistry 45*, 6529−6540.
32. Hetru, C., Letellier, L., Oren, Z., Hoffmann, J. A., and Shai, Y. (2000) Androctonin, a hydrophilic disulfide-bridged non-haemolytic anti-microbial peptide: A plausible mode of action, *Biochem. J. 345*, 653−664.
33. Buffy, J. J., Hong, T., Yamaguchi, S., Waring, A., Lehrer, R. I., and Hong, M. (2003) Solid-State NMR Investigation of the Depth of Insertion of Protegin-1 in Lipid Bilayers Using Paramagnetic Mn^{2+}, *Biophys. J. 85*, 2363−2373.
34. Sinha, N., Schmidt-Rohr, K., and Hong, M. (2004) Compensation for Pulse Imperfections in Rotational-Echo Double-Resonance NMR by Composite Pulses and EXORCYCLE, *J. Magn. Reson. 168*, 358−365.

BI061424U